PNAS RESEARCH ARTICLE | BIOCHEMISTRY

Regulation mechanisms of the dual ATPase in KaiC

Yoshihiko Furuike[a,b], Atsushi Mukaiyama[a,b], Shin-ichi Koda[c], Damien Simon[a,b], Dongyan Ouyang[a], Kumiko Ito-Miwa[d], Shinji Saito[c], Eiki Yamashita[e], Taeko Nishiwaki-Ohkawa[f,g], Kazuki Terauchi[h,i], Takao Kondo[d], and Shuji Akiyama[a,b,1]

Edited by Carl Johnson, Vanderbilt University, Nashville, TN; received October 29, 2021; accepted March 28, 2022 by Editorial Board Member Michael Rosbash

KaiC is a dual adenosine triphosphatase (ATPase), with one active site in its N-terminal domain and another in its C-terminal domain, that drives the circadian clock system of cyanobacteria through sophisticated coordination of the two sites. To elucidate the coordination mechanism, we studied the contribution of the dual-ATPase activities in the ring-shaped KaiC hexamer and these structural bases for activation and inactivation. At the N-terminal active site, a lytic water molecule is sequestered between the N-terminal domains, and its reactivity to adenosine triphosphate (ATP) is controlled by the quaternary structure of the N-terminal ring. The C-terminal ATPase activity is regulated mostly by water-incorporating voids between the C-terminal domains, and the size of these voids is sensitive to phosphoryl modification of S431. The up-regulatory effect on the N-terminal ATPase activity inversely correlates with the affinity of KaiC for KaiB, a clock protein constitutes the circadian oscillator together with KaiC and KaiA, and the complete dissociation of KaiB from KaiC requires KaiA-assisted activation of the dual ATPase. Delicate interactions between the N-terminal and C-terminal rings make it possible for the components of the dual ATPase to work together, thereby driving the assembly and disassembly cycle of KaiA and KaiB.

circadian clock | cyanobacteria | KaiC | ATPase | structure

Significance

KaiC, a core clock protein in the cyanobacterial circadian clock system, hydrolyzes adenosine triphosphate (ATP) at two distinct sites in a slow but ordered manner to measure the circadian timescale. We used biochemical and structural biology techniques to characterize the properties and interplay of dual-adenosine triphosphatase (ATPase) active sites. Our results show that the N-terminal and C-terminal ATPases communicate with each other through an interface between the N-terminal and C-terminal domains in KaiC. The dual-ATPase sites are regulated rhythmically in a concerted or opposing manner dependent on the phase of the circadian clock system, controlling the affinities of KaiC for other clock proteins, KaiA and KaiB.

The circadian clock is an endogenous timekeeping system that rhythmically controls a variety of biological phenomena with a period of about 24 h. The rhythms of the circadian clock remain stable without external stimuli even under homeostatic conditions (self-sustained oscillation), and their period is kept constant even when the ambient temperature changes (temperature compensation). Moreover, the circadian clock system responds by shifting its internal phase back and forth depending on external stimuli, such as light and temperature, and through this phase response, the internal phase of the timing system can be synchronized with the external phase of the environmental cycle (synchronization). These unique properties allow organisms to adapt to the daily environmental cycles on Earth.

KaiC is a core clock protein that regulates the circadian rhythm of the cyanobacterium *Synechococcus elongatus* PCC (Pasteur culture collection) 7942 (1). This protein utilizes two types of adenosine triphosphate (ATP) molecules to produce diverse chemical reactions and thereby, generate a temperature-compensated circadian rhythm (2–4). ATP molecules bind to a Walker motif present in two tandemly replicated domains, specifically N-terminal C1 and C-terminal C2 domains (Fig. 1*A*). The binding of ATP triggers the oligomerization of KaiC into a double-ring hexamer (5) (Fig. 1*A*). The ATP molecule bound to the C2 domain (C2-ATP) is the primary source of a phosphoryl group that is transferred to S431 and T432 of KaiC (autokinase) and then removed (autophosphatase) (6, 7). In the presence of KaiA and KaiB, the state of the phosphorylation sites changes periodically even in vitro (6–8): ST → SpT → pSpT → pST → ST, where S, T, pS, and pT represent S431, T432, phosphorylated S431, and phosphorylated T432, respectively. In addition, it has been suggested that a small amount of C2-ATP is hydrolyzed into adenosine diphosphate (C2-ADP) as adenosine triphosphatase (C2-ATPase) via a complicated reaction scheme (9, 10). On the other hand, the frequency of the phosphorylation cycle is proportional to the hydrolysis (C1-ATPase) rate of C1-bound ATP (C1-ATP) in the absence of KaiA and KaiB (11, 12). The C1-ATPase activity greatly exceeds the C2-ATPase activity under steady state and is temperature compensated (12). Overall ATPase activities, including those of C1 and C2 (C1/C2-ATPase), are known to oscillate with the circadian period (12) in the presence of KaiA and KaiB (Fig. 1*B*) and also, to reveal a damping oscillatory relaxation even without KaiA and KaiB (11).

The C1/C2-ATPase of KaiC is an important research target to achieve a better understanding of the circadian clock system in cyanobacteria (3), as it closely relates to oscillatory, period-tuning, and temperature-compensating properties. Although much effort has been devoted to the biochemical (12–18) and structural analyses (11, 19–21)

Author contributions: Y.F. and S.A. designed research; Y.F., A.M., D.S., D.O., and E.Y. performed research; K.I.-M., T.N.-O., K.T., and T.K. contributed new reagents/analytic tools; Y.F., S.-i.K., S.S., and S.A. built mathematical models; Y.F. and S.A. analyzed data; and Y.F., S.-i.K., and S.A. wrote the paper.

The authors declare no competing interest.

This article is a PNAS Direct Submission. C.J. is a guest editor invited by the Editorial Board.

[1]To whom correspondence may be addressed. Email: akiyamas@ims.ac.jp.

This article contains supporting information online at http://www.pnas.org/lookup/suppl/doi:10.1073/pnas.2119627119/-/DCSupplemental.

Published May 4, 2022.

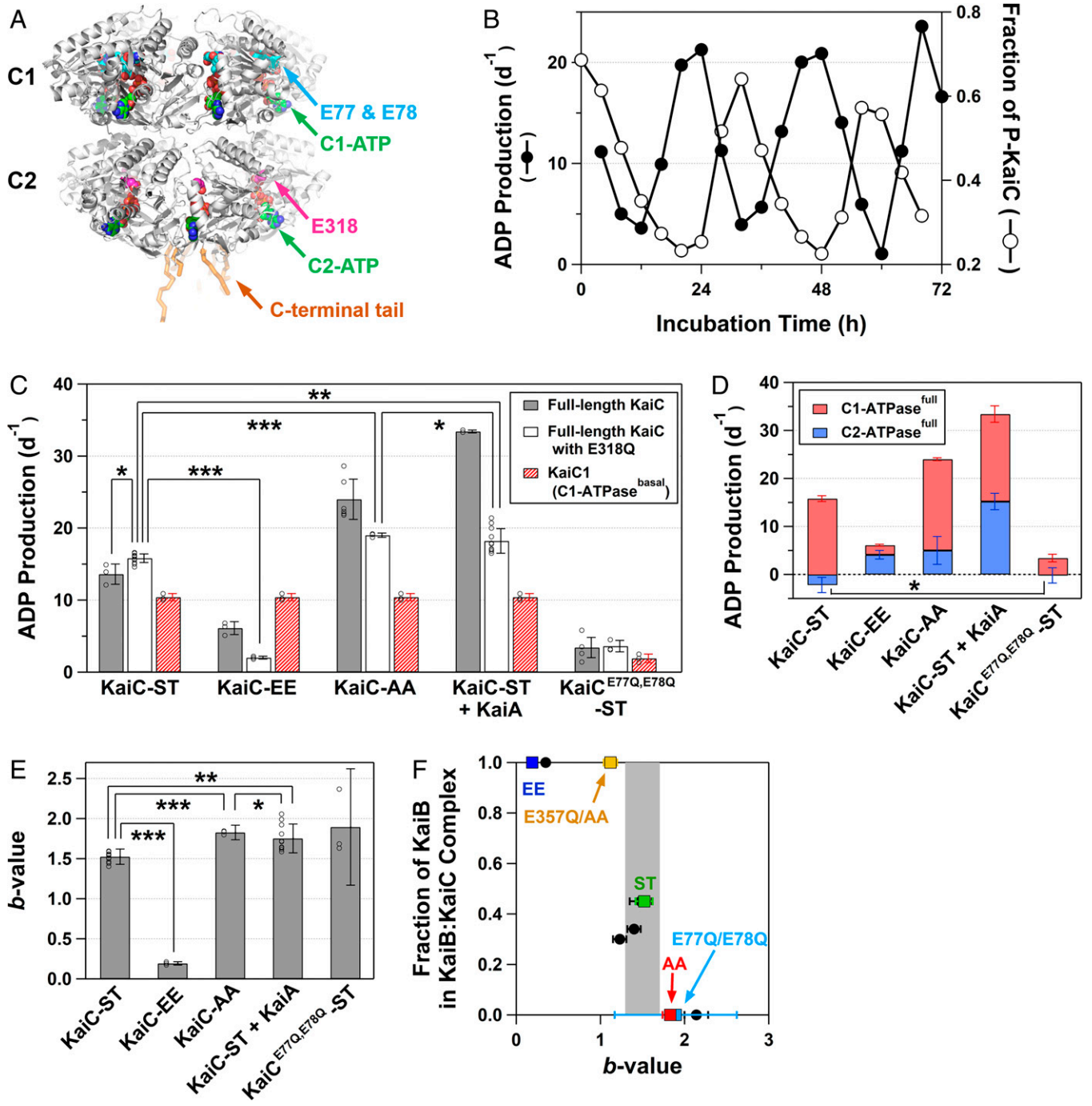

Fig. 1. Regulation of the dual C1/C2-ATPase in KaiC. (*A*) Active sites of the dual C1/C2-ATPase in the KaiC hexamer (5). (*B*) Rhythmic changes in the C1/C2-ATPase activity of KaiC (left axis) and the fraction of phosphorylated KaiC (P-KaiC; right axis) in the presence of KaiA and KaiB at 30 °C. (*C*) Measured rates of ADP production. Gray, white, and hatched bars represent the ATPase activities of full-length KaiCs (contributions from C1 and C2), full-length KaiCs carrying the E318Q substitution (contribution from C1), and truncated KaiCs (KaiC1) consisting solely of the C1 domain (C1-ATPase^{basal}; C1 basal activity without the C2 domains). ATPase activities were assayed by measuring ADP production for 10 to 16 h. In the case of KaiC-ST (0.20 mg/mL) + KaiA (0.12 mg/mL), data are given as apparent activities estimated by the ADP production for 10 h. The ATPase activities were analyzed using one-way ANOVA ($F_{4,28} = 2.714$, $P = 2.30 \times 10^{-17}$) and the Bonferroni post hoc *t* test. *Insignificant ($P > 0.05/10$); **significant ($P < 0.005/10$); ***significant ($P < 0.0005/10$). (*D*) Calculated rates of ADP production in the C1 (C1-ATPase^{full}; red bars) and C2 domains (C2-ATPase^{full}; blue bars) of the full-length KaiCs. C1-ATPase^{full} indicates ATPase activity of full-length KaiCs carrying the E318Q substitution (white bars in *C*). C2-ATPase^{full} indicates ATPase activity of full-length KaiCs (gray bars in *C*) minus C1-ATPase^{full} (white bars in *C*). *Insignificant ($P > 0.05$): *t* test of C2-ATPase^{full}. (*E*) The *b* values defined as the ratio of C1-ATPase^{full} (red bars in *D*) to C1-ATPase^{basal} (hatched bars in *C*) (details are in Eq. **1** and *Materials and Methods*). The *b* values were analyzed using one-way ANOVA ($F_{3,26} = 2.975$, $P = 3.95 \times 10^{-17}$) and the Bonferroni post hoc *t* test. *Insignificant ($P > 0.05/6$); **significant ($P < 0.005/6$); ***significant ($P < 0.0005/6$). (*F*) Potential correlation between *b* value and KaiB–KaiC affinity. The fraction of KaiB forming KaiB–KaiC complexes was determined by native PAGE analysis (*SI Appendix*, Fig. S3*A*). C1/C2-ATPase and *b* values for a series of mutants (black circles) are compiled in *SI Appendix*, Table S3.

of KaiC ATPase, the mechanisms of its activation and inactivation remain unknown. In this study, we measured the contributions of C1-ATPase and C2-ATPase separately by introducing amino acid substitutions in KaiC. Then, we attempted to estimate and parameterize the degree to which C1-ATPase is activated and inactivated by the C2 domain. Furthermore, we performed a crystal structure analysis of the activated and inactivated forms of KaiC. Our results suggest that the components

of the dual ATPase communicate with each other through C1–C2 interaction to control the assembly and disassembly cycle of KaiA and KaiB.

Results

Contributions of C1- and C2-ATPases. The steady-state C1/C2-ATPase activity of fully dephosphorylated KaiC (KaiC-ST) was 13.6 ± 1.4 d^{-1} at 30 °C (gray bars in Fig. 1*C*). To estimate the contribution of C1-ATPase in full-length KaiC (C1-ATPase^{full}), we inactivated the kinase and C2-ATPase by replacing the catalytic glutamate 318 with glutamine (13–16, 22). The resultant KaiC^{E318Q}-ST exhibited a measured activity of 15.8 ± 0.6 d^{-1} (white bars in Fig. 1*C*), which was comparable with the activity of KaiC-ST. Given that this measured activity of KaiC^{E318Q}-ST reflects the C1-ATPase^{full} activity of KaiC-ST (red bars in Fig. 1*D*), the contribution of C2-ATPase^{full} can be estimated as the difference in the measured activities between KaiC-ST and KaiC^{E318Q}-ST, which was as small as −2.2 ± 1.6 d^{-1} (blue bars in Fig. 1*D*). On the other hand, the ATPase activity of a truncated KaiC (KaiC1) consisting solely of the C1 domain (11), which reflects the basal activity of the C1-ATPase (C1-ATPase^{basal}) without the influence of the C2 domain, was 10.4 ± 0.5 d^{-1} (hatched bars in Fig. 1*C*).

The regulatory effect of the C2 domain on C1-ATPase^{full} was evaluated using a parameter (*b* value) defined as the ratio of C1-ATPase^{full} to C1-ATPase^{basal} by the following equation:

$$b\ \text{value} = \text{C1}-\text{ATPase}^{full}/\text{C1}-\text{ATPase}^{basal}, \qquad [1]$$

where C1-ATPase^{full} and C1-ATPase^{basal} correspond to the ATPase activities of full-length KaiC with the E318Q substitution and truncated KaiC consisting solely of the C1 domain, respectively. The *b* value was 1.52 ± 0.10 for KaiC-ST (Fig. 1*E*), reflecting the up-regulation of its C1-ATPase by the C2 domain. These results suggest that the C1-ATPase^{full} activity in KaiC-ST is ∼50% up-regulated by the C2 domain (Fig. 1*E*), while the contribution of the C2-ATPase^{full} in KaiC-ST is negligibly small (Fig. 1*D*). It must be noted that we did not rely on an alternative strategy of inactivating C1-ATPase by corresponding E77Q/E78Q mutations (13–16) to estimate the contribution of C2-ATPase, as KaiC^{E77Q,E78Q}-ST and even KaiC1^{E77Q,E78Q} exhibited residual C1-ATPase activity as high as 3.4 ± 1.4 and 1.9 ± 0.6 d^{-1}, respectively (Fig. 1*C* and *SI Appendix, Supplementary Text*).

To investigate how phosphoryl modifications affected C1/C2-ATPase, we measured the activity of a KaiC-pSpT–mimicking S431E/T432E KaiC mutant (KaiC-EE). The C1-ATPase^{full} and C2-ATPase^{full} activities of KaiC-EE were 2.0 ± 0.2 and 4.1 ± 0.9 d^{-1}, respectively (Fig. 1*D*). The *b* value of KaiC-EE was estimated to be 0.19 ± 0.02, indicating 80% down-regulation of its C1-ATPase^{full} (Fig. 1*E*). By contrast, an S431A/T432A KaiC mutant (KaiC-AA), which may be treated as a phosphomimic mutant of KaiC-ST, exhibited an elevated activity of 24.0 ± 2.8 d^{-1} (Fig. 1*C*) as reported previously (12). While the C2-ATPase^{full} activity of KaiC-AA was 5.0 ± 2.9 d^{-1}, which was comparable with that of KaiC-EE (4.1 ± 0.9 d^{-1}) (Fig. 1*D*), the C1-ATPase^{full} activity was 80% up-regulated as high as 19.0 ± 0.3 d^{-1} (*b* = 1.83 ± 0.09 in Fig. 1*E*). The excessive activation of C1/C2-ATPase in KaiC-AA relative to KaiC-ST indicates that KaiC-AA is not an exact functional counterpart of KaiC-ST.

We found that KaiC-AA is rather similar to a KaiA-stimulated state of KaiC-ST. KaiA was previously shown to activate the ATPase activity of KaiC (12). Consistent with that study, the addition of KaiA to KaiC-ST resulted in the activation of the dual ATPase. The C1-ATPase^{full} activity of KaiA-stimulated KaiC-ST was 18.2 ± 1.7 d^{-1} (Fig. 1*D*), and it was ∼80% up-regulated relative to KaiC-ST alone (*t* test: **significant, $P < 0.005/10$ in Fig. 1*C* and *b* = 1.75 ± 0.18 in Fig. 1*E*). The contribution of C2-ATPase^{full} in KaiC-ST became very obvious in the presence of KaiA, with enhanced activity of 15.2 ± 1.7 d^{-1} for the initial 10 h (Fig. 1*D*). These observations suggest that the KaiA stimulation of C1/C2-ATPase of KaiC-ST is mimicked in KaiC-AA even without KaiA.

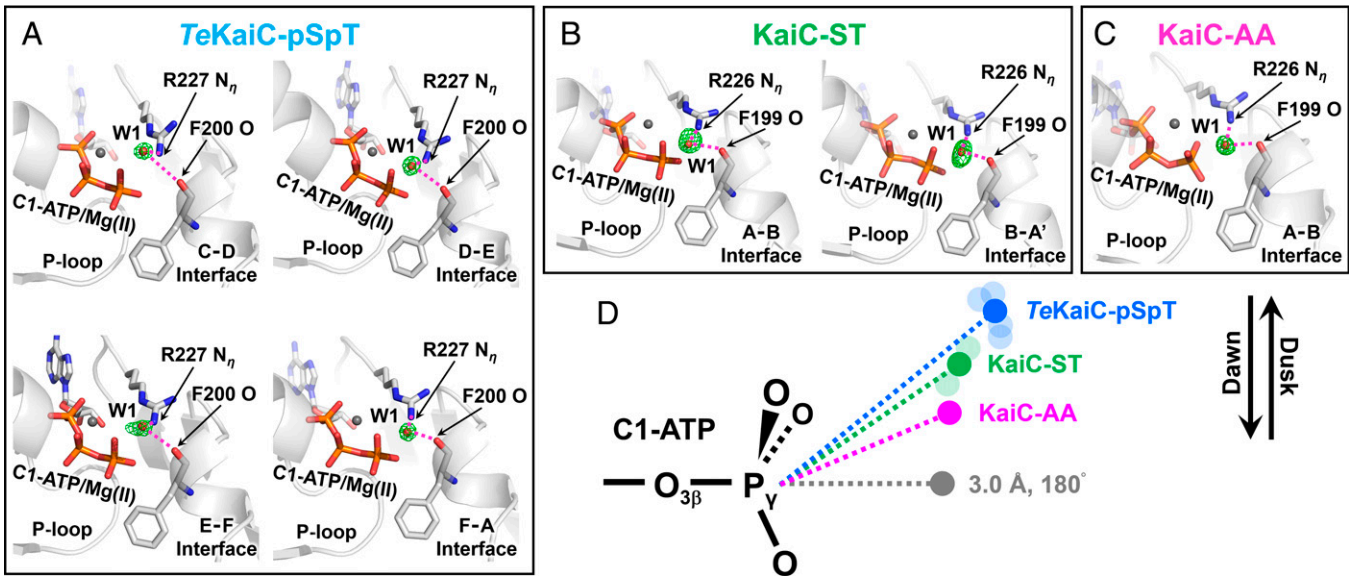

Fig. 2. Active site structures of C1-ATPase in KaiC. W1 (red spheres) identified for (*A*) *Te*KaiC-pSpT, (*B*) KaiC-ST, and (*C*) KaiC-AA. The difference Fourier (*Fo*–*Fc*) omit maps (green mesh) in *A*–*C* are contoured as follows: 3.0σ, 5.0σ, 2.8σ, and 2.6σ; 3.3σ and 2.0σ; and 4.0σ, respectively. W1s are sequestered through hydrogen bonds (magenta dotted lines) by F199 and R226 (F200 and R227 in *Te*KaiC) to regulate their position relative to the ATP molecule bound to the C1 domain. (*D*) Schematic drawing of dawn- and dusk-phase repositioning of W1 (*SI Appendix*, Table S2). Dark-colored circles correspond to the mean W1 positions from independent C1–C1 interfaces (pale-colored circles).

Structural Basis for Up- and Down-Regulation of C1-ATPase^{full}. ATP hydrolysis includes a reaction step in which a lytic water molecule (W1) attacks the phosphorus atom (P_γ) of the terminal γ-phosphate of ATP. Thus, the relative positioning of W1 and P_γ is one of the crucial factors determining the reaction efficiency, as reported previously (11). To investigate the W1 position, we sought to crystallize KaiC-AA (*SI Appendix*, Table S1) and to compare the results with those for KaiC-ST and KaiC-pSpT, which we previously reported (23). We could identify a reasonable electron density for W1 in all cases (Fig. 2 *A*–*C* and *SI Appendix*, Table S2), except for KaiC-pSpT. Fortunately, however, another 2.2-Å crystal structure of thermophilic KaiC from *Thermosynechococcus elongatus* (*Te*KaiC) was determined in the *Te*KaiC-pSpT state (*SI Appendix*, Table S1), with a clear electron density for W1.

In *Te*KaiC-pSpT (Fig. 2*A*), W1 was hydrogen bonded to the carbonyl oxygen atom of F200 and R227 N_η (F199 and R226 in KaiC) and sequestered at the position most unfavorable for S_N2-type ATP hydrolysis, with a W1–P_γ distance of 5.1 Å and a W1–P_γ–$O_{3\beta}$ angle of 141° (Fig. 2*D*). By contrast, W1 was located at a less unfavorable position in KaiC-ST (Fig. 2*B*), with a shorter W1–P_γ distance (4.0 Å) and a larger W1–P_γ–$O_{3\beta}$ angle (147°) (Fig. 2*D*). W1 was found in positions more suitable for ATP hydrolysis in KaiC-AA (Fig. 2 *C* and *D*). The descending and ascending orders of the W1–P_γ distance and the W1–P_γ–$O_{3\beta}$ angle (Fig. 2*D*), respectively, matched the increasing order of the C1-ATPase^{full} activity (KaiC-EE[pSpT] < KaiC-ST < KaiC-AA) (Fig. 1 *C* and *D*). These results confirm that the relative positioning of W1 and P_γ is one of the factors impacting up- and down-regulation of C1-ATPase^{full}.

Structural Basis for Up- and Down-Regulation of C2-ATPase^{full}. The electron densities for W1s involved in C2-ATPase could not be identified in the crystal structures of KaiC-pSpT, *Te*KaiC-pSpT, KaiC-ST, or KaiC-AA, possibly due to their dynamic nature. On the other hand, we found unique variation patterns in a tunnel-shaped void in the C2–C2 interface (Fig. 3), through which bulk water molecules migrate to the C2-ATPase active site.

In KaiC-ST, the distal side of the γ-phosphate of C2-ATP is stereochemically crowded by several residues (E318, S431, and T432) and consequently, does not have enough space to stably accommodate any water molecules (Fig. 3 *A*, *Inset*). Although a tunnel-shaped void was confirmed near the distal side, it was undulated (Fig. 3*A*) and too narrow (Fig. 3*D*) to freely take up water molecules (radius of ∼1.4 Å) from the inner-radius side of the hexamer. The corresponding water tunnels were not uniform within the KaiC-pSpT hexamer (*SI Appendix*, Fig. S1), but the shortest one suggests more effective uptake by KaiC-pSpT than by KaiC-ST (Fig. 3 *B* and *D*). By contrast, the distal side of KaiC-AA was more relaxed. A wider straight channel

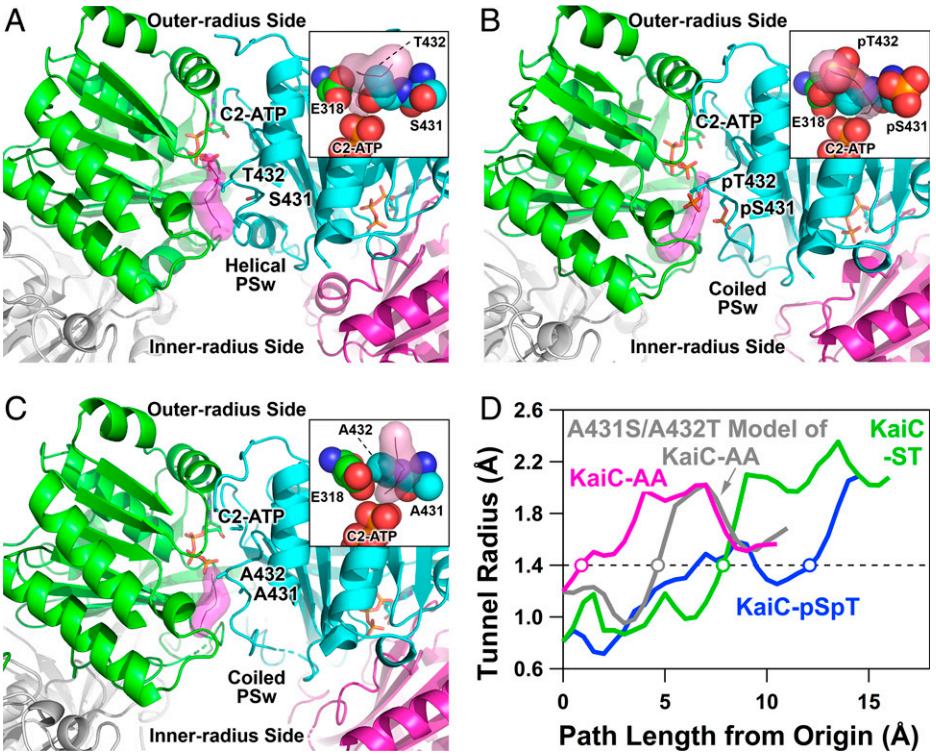

Fig. 3. Tunnel-shaped voids extending along C2–C2 interfaces from C2-ATP to the inner-radius side of the hexamer. Zoomed-in view of C2–C2 interfaces for (*A*) KaiC-ST, (*B*) KaiC-pSpT, and (*C*) KaiC-AA. Tunnels (magenta surface) extend from the vicinity of P_γ of C2-ATP to the inner-radius side of the hexamer. *A*, *Inset*, *B*, *Inset*, and *C*, *Inset* depict representative amino acids, shown as space-filling models, located on the distal side of the γ-phosphate of C2-ATP. (*D*) Radius of the tunnels as a function of path length from the origin (near P_γ of C2-ATP). The shortest and widest tunnels in KaiC-ST, KaiC-pSpT, KaiC-AA, and an A431S/A432T model of KaiC-AA (*SI Appendix*, Fig. S2) are shown by green, blue, magenta, and gray lines, respectively. Note that the diversity of tunnel shapes at each protomer interface is more pronounced in KaiC-pSpT (*SI Appendix*, Fig. S1). Open circles correspond to the point where the tunnel radius first falls below the radius of a water molecule (1.4 Å; dashed line in *D*). The traces of KaiC-AA and the A431S/A432T model of KaiC-AA are terminated at the path length of ∼10 Å because their tunnels are shorter by ∼5 Å than those in other KaiCs. In KaiC-ST, the first half of the tunnel is undulated (thick black line in *A*, *Inset*) and then narrowed by bottleneck residues down to a radius of ∼0.8 Å, far smaller than the radius of the water molecule. Thus, the tunnel of KaiC-ST is not wide enough to freely take up water molecules from the inner-radius side. By contrast, the tunnel without a bottleneck that exhibits straight extension in KaiC-AA is ready to transfer water molecules from the inner-radius side to the active site of C2-ATPase. The modeling of A431S/A432T using the KaiC-AA template results in a narrowing of the tunnel radius at the path length of around 3 Å, but neither the total length of the tunnel nor the radius near the origin are affected at all.

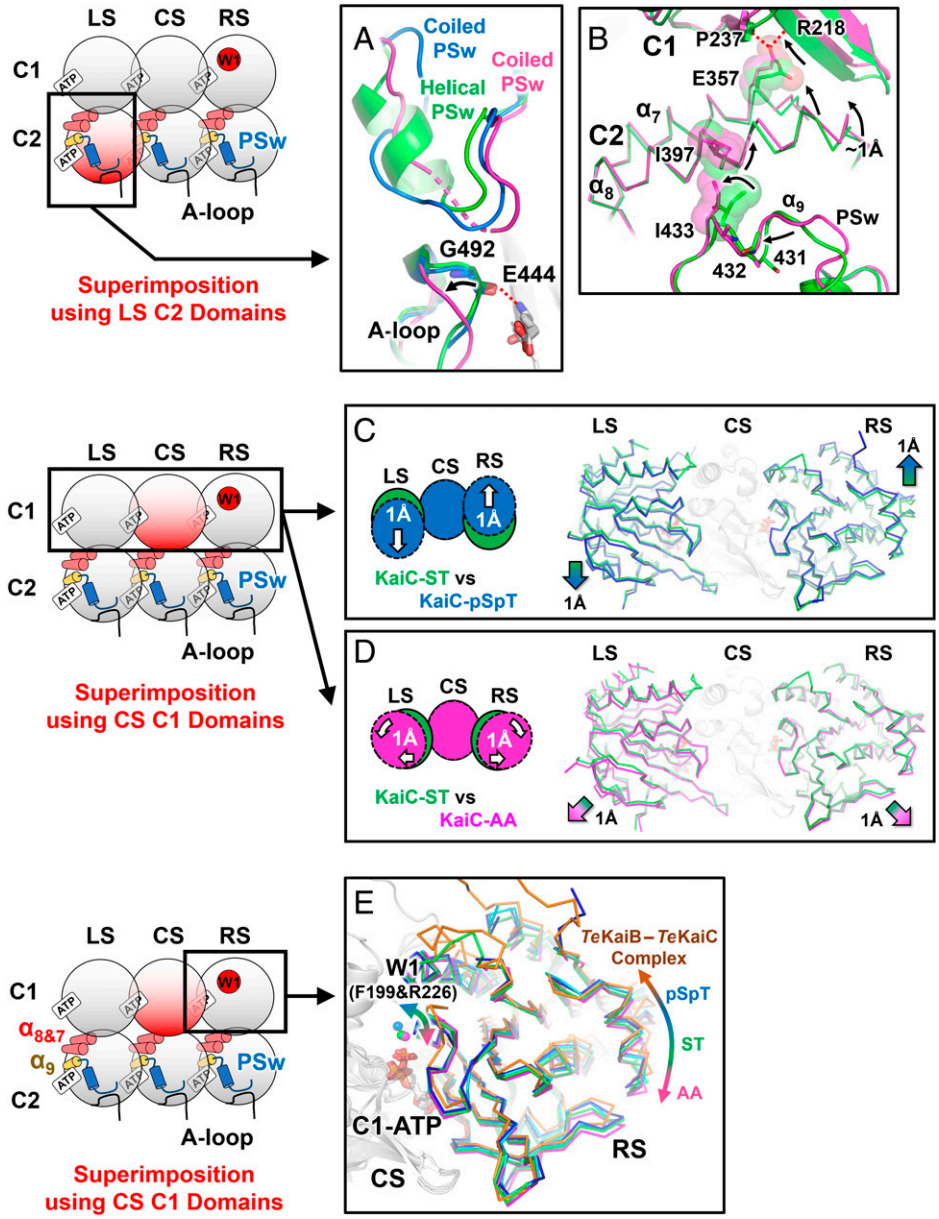

Fig. 4. Up- and down-regulation of C1-ATPase via quaternary structural changes. KaiC-ST (green), KaiC-pSpT (blue), and KaiC-AA (magenta) crystal structures are viewed from the inner-radius side of the hexamer and superimposed using a red-colored C1 or C2 domain of center subunit (CS), right subunit (RS), or left subunit (LS) as shown in schematic diagrams. (*A*) Helix to coil transition of PSw and unfolding of A loop in the transition from KaiC-ST to KaiC-AA. The hydrogen bond between G492 and E444 observed in KaiC-ST is disrupted in KaiC-AA. (*B*) C1-ring quaternary structural change assisted by positional shifts of PSw, α_9, α_8, and α_7 in KaiC-AA. α_8 is lifted up toward the C1 domain by steric contacts between I433 and I397. (*C*) Tilt and slide movement of the C1 domain in KaiC-pSpT. (*D*) Outer radius–directed movement of the C1 domain to form a less compact C1 ring of KaiC-AA. (*E*) Sliding of the C1–C1 interface and updating of lytic water (W1) positions. KaiC-pSpT (blue), *Te*KaiC-pSpT (cyan), KaiC-ST (green), KaiC-AA (magenta), and *Te*KaiC-ET (brown) complexed with *Te*KaiB (5JWQ) (30) are superimposed using their C1 domains in the CS subunit. Note that the affinity of KaiC for KaiB is reduced (Fig. 1*F*) as the relative position of the RS–C1 domain to the CS–C1 domain shifts in the C2 direction.

(Fig. 3*C*) connected the space in the distal side to the exterior of the hexamer and appeared to allow effective migration of water molecules into the active site of C2-ATPase (Fig. 3*D*). Furthermore, the side chain of catalytic E318 was positioned at one end of the water tunnel and could immediately activate the migrated water molecules (Fig. 3 *C*, *Inset*). The descending and ascending orders of the path length and width of the tunnel-shaped voids, respectively, approximately matched the increasing order of the C2-ATPase^{full} activity (KaiC-ST < KaiC-EE[pSpT] < KaiC-AA) (Fig. 1 *C* and *D*). These observations provide a structural explanation for why C2-ATPase is down-regulated in KaiC-ST but up-regulated in KaiC-EE and KaiC-AA.

To evaluate local effects of the S431A/T432A substitutions that intrinsically reduce the volume of the side chains, we constructed an A431S/A432T model using the main chain structure of KaiC-AA as a template (*SI Appendix*, Fig. S2). While a partial decrease in the tunnel radius at the path length of around 3 Å was observed (gray line in Fig. 3*D*), neither the total length of the tunnel nor the radius at the origin were affected at all, and the position where the tunnel radius first became below the radius of the water molecule was sufficiently closer to the origin than that of KaiC-ST and KaiC-pSpT (open circles in Fig. 3*D*). The efficient uptake of the water molecules into C2-ATP in KaiC-AA can be attributed to the local reduction of the side-chain volume by the dual alanine substitutions and to other nonlocal structural changes that shorten the tunnel length and enlarge the radius around the origin.

Quaternary Structural Changes. A region upstream of the dual-phosphorylation sites in the C2 domain called phosphor switch (PSw) (23) adopts coiled and helical conformations in KaiC-pSpT (EE) and KaiC-ST, respectively (Fig. 4*A*). Our previous study (23) suggested that this fold switch of PSw influences the quaternary structure of the C1 ring through the C1–C2 interface. When superimposed using the C1 domains of KaiC-pSpT and KaiC-ST as references (Fig. 4*C*), one of the two adjacent C1 domains (right subunit in Fig. 4*C*) of KaiC-pSpT shifted by ∼1 Å away from the C2 domain, but conversely, the other C1 domain (left subunit in Fig. 4*C*) shifted toward the C2 domain. These observations indicate that during the helix to coil transition of PSw from KaiC-ST to KaiC-pSpT, every C1 domain gently tilts and then leans over a neighboring C1 domain (Fig. 4*C*). This tilting and sliding movement causes W1, which is sequestered by F199 and R226 (F200 and R227 in *Te*KaiC), to move one position further toward the ATP molecule bound to the C1 domain (Figs. 2*D* and 4*E*).

PSw of KaiC-AA was found to adopt a loop conformation (Fig. 4*A*), providing the tunnel-shaped void in the C2–C2 interface to allow uptake of bulk water molecules to the C2-ATPase active site (Fig. 3 *C* and *D*). Compared with KaiC-ST, the coiled PSw of KaiC-AA was shifted away from the nearest C2-ATP, similar to what was observed in KaiC-pSpT (Fig. 4*A*). However, the effects of these PSw shifts on two adjacent α-helices (α_8 and α_7) were slightly but notably different between KaiC-AA and KaiC-pSpT. In KaiC-AA, the short helix (α_9) located downstream of PSw was shifted to the outer-radius side of the hexamer, and the resultant steric hindrance between I433 (α_9) and I397 (α_8) pushed the N terminus of α_8 toward the C1 direction by ∼1 Å (Fig. 4*B*). Concomitantly, α_7 placed in parallel to α_8 was pushed in the same direction. The side chain of E357 (α_7) was hydrogen bonded to P237 and R218 in the C1 domain, and it was inserted into the C1 side as α_7 changed its orientation. These positional shifts of PSw, α_9, α_8, and α_7 in KaiC-AA assist the movement of every C1 domain to the outer-radius side by ∼1 Å (Fig. 4*D*), finally shifting W1 in every C1–C1 interface into a position more suitable for ATP hydrolysis (Fig. 2*D*) and thus, further activating C1-ATPase (*t* test: ***significant, $P < 0.0005/6$; **significant, $P < 0.005/6$ in Fig. 1*E*).

Coiled and shifted PSw also influenced the C-terminal region of KaiC-AA. Amino acids positioned from 488 to 497 form a loop (A loop) (24) in both KaiC-ST and KaiC-pSpT, but the loop is deformed in KaiC-AA to allow its KaiA-binding C terminus (498 to 519) (25) to be more exposed to solvent (Fig. 4*A*). This observation is consistent with those of previous studies (26, 27) that reported a high affinity of KaiA to KaiC-AA, implying that the structure of KaiC-AA reflects the KaiA-stimulated or KaiA-postbound state of KaiC-ST. Consistent with the expectation that the A loop is pulled down by KaiA binding to the C terminus of KaiC-ST (24), a key hydrogen bond between G492 and E444 is disrupted in KaiC-AA (Fig. 4*A*).

Relationship between the Regulatory State of C1-ATPase^{full} and KaiB Affinity. It has been shown that KaiB binds to the C1 domain of KaiC (28–30), and the affinity and kinetics of the KaiB–KaiC interaction have been investigated in detail (31, 32). To evaluate the functional significance of the observed quaternary structural changes of the C1 ring (Fig. 4 *C*–*E*), we studied the affinity of KaiC to KaiB with native polyacrylamide gel electrophoresis (PAGE) analyses. A mixture of equimolar amounts of KaiB and KaiC-ST (5 μM on a monomer basis) after incubation at 30 °C for 30 h revealed that 50% of KaiB bound to KaiC-ST (>97% dephosphorylation) to form a KaiB–KaiC-ST binary complex (*SI Appendix*, Fig. S3*A*). Interestingly, as summarized in Fig. 1*F*, the KaiB affinity of a series of KaiC mutants revealed a correlation with the *b* value; the affinity of KaiC for KaiB decreased as the *b* value increased (*SI Appendix*, Fig. S3*A* and Table S3). This correlation suggests that the C1-ring status responsible for KaiB binding switches in the range of *b* values between ∼1.3 and 1.7. While the *b* value of KaiC-ST was in the transition region, the affinity of KaiC-AA for KaiB was below the present limit of detection by native PAGE, as reported previously (6, 33, 34). Astonishingly, as long as the rules for up- and down-regulation are satisfied, KaiC could dramatically switch even from extremely low-affinity (KaiC-AA) to high-affinity forms (KaiC^{E357Q}-AA). In this context, KaiC-AA is a poor mimic of KaiC-ST in terms of not only structure (Figs. 2 and 3) but also, KaiB binding (Fig. 1*F*). Our results clearly indicate that the C1-ATPase^{full} of KaiC-ST is not up-regulated enough to completely disrupt the interaction between KaiB and KaiC-ST (Fig. 1*F*).

The complete disassembly of KaiB from KaiC requires the KaiA-assisted activation of the dual ATPase. Immediately after the addition of KaiA ($t = 0$ h) to the KaiB–KaiC-ST complex that was preformed for 48 h (black line in Fig. 5*A*), KaiA was trapped on KaiB interacting with the C1 domain of KaiC-ST and then eluted from a size-exclusion chromatography (SEC) column as the KaiA–KaiB–KaiC-ST ternary complex ($t = 0$) (Fig. 5*A*). Within 1.5 h at 30 °C, the peak intensity of the ternary complex decreased, whereas that of free KaiB increased (Fig. 5 *A*, *Inset*), and the dual-phosphorylation site of KaiC-ST remained unchanged (Fig. 5*C*). By contrast, more ADP was produced by the KaiA/KaiB/KaiC-ST mixture than by the KaiB/KaiC-ST mixture within 1.5 h, peaking ∼4 h after the KaiA addition (Fig. 5*D*). A small amount of free KaiA (Fig. 5*E* and *SI Appendix*, Fig. S3*B*) likely binds the C-terminal loop of KaiC-ST and then activates ATPase to disrupt the interaction between KaiB and KaiC-ST (31), as a KaiC mutant (KaiC$^{\Delta 505}$) lacking the C terminus (506 to 519) (19, 24, 33) was assembled into a KaiA–KaiB–KaiC$^{\Delta 505}$-ST complex that rarely disassembled (Fig. 5*B*). These results are qualitatively consistent with the earlier observation (35) that KaiB and KaiC-EE are prevented from forming the complex in the presence of an excessive amount of KaiA. Notably, the KaiA-assisted disassembly shown in Fig. 5 has the appearance of an autocatalytic reaction often found in oscillators; a KaiA molecule released from a ternary complex can react with another ternary complex to promote the release of another KaiA molecule (*SI Appendix*, Fig. S4*F*).

To examine this hypothesis, we conducted a preliminary mathematical model analysis of the KaiA-assisted disassembly. Our present model provides only a qualitative assessment because it does not take into consideration KaiB rebinding to the KaiC hexamer (*SI Appendix*, *Extended Methods*). Nevertheless, important aspects of our experimental observations were reflected by the model when optimized parameter values were used. First, the disassembly of the KaiA–KaiB–KaiC-ST complex preceded the accumulation of phosphorylated KaiC (Fig. 5 *A* and *C* and *SI Appendix*, Fig. S4*A*). Second, free KaiB accumulated ∼4 h before free KaiA increased (Fig. 5*E* and *SI Appendix*, Fig. S4*B*). Third, the concentration of the KaiA–KaiC complex peaked at ∼4 h (*SI Appendix*, Fig. S4*A*), when the time-dependent increase in KaiC-SpT abundance was maximized (Fig. 5*C*). Fourth, the present model (*SI Appendix*, Fig. S4*D*) successfully predicted the KaiA-dependent acceleration of disassembly and phosphorylation dynamics (*SI*

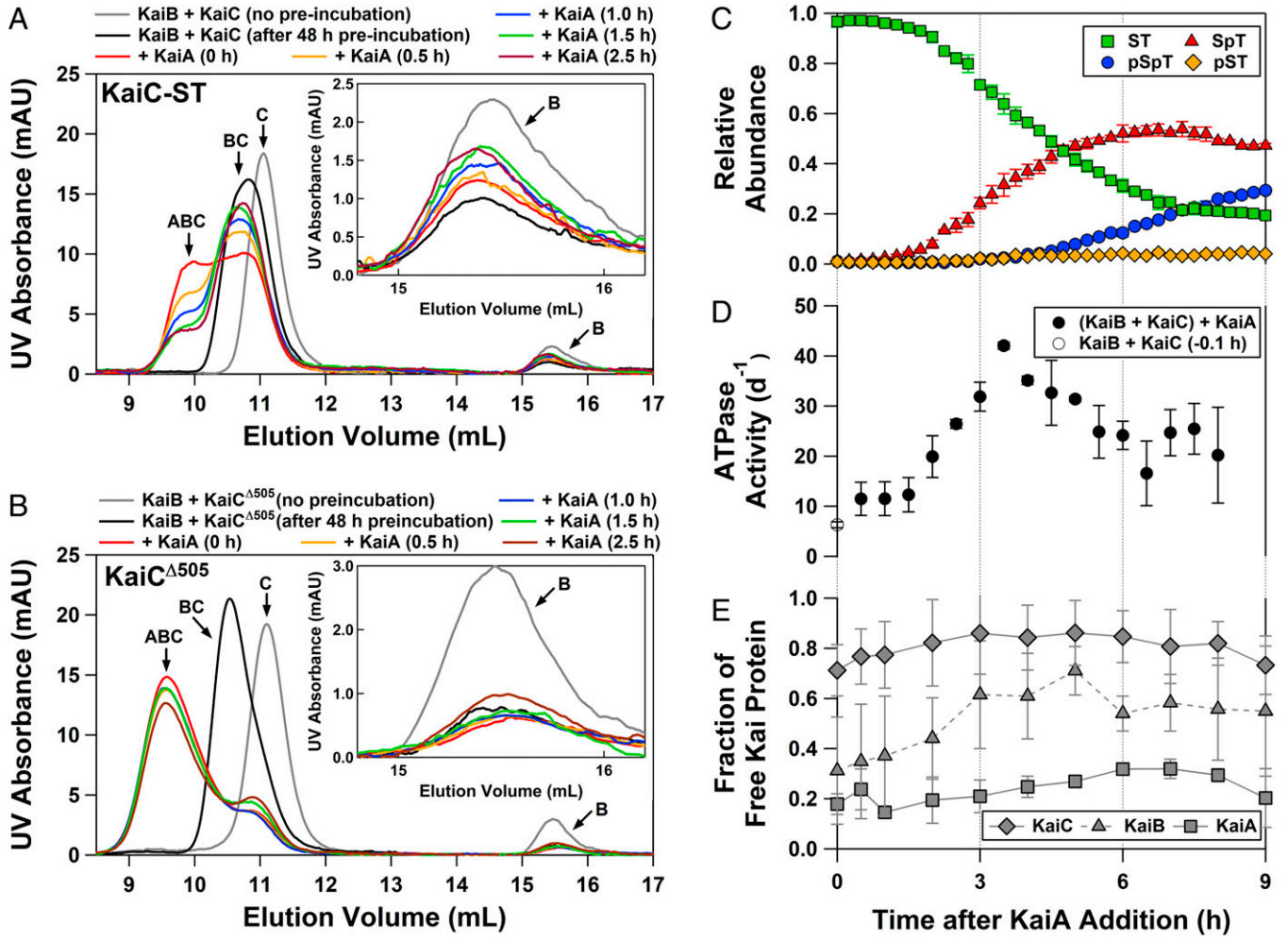

Fig. 5. Activated C1/C2-ATPase of KaiC triggers disassembly of the KaiABC ternary complex. Time evolution of SEC chromatograms before and after adding KaiA to the preformed (*A*) KaiB–KaiC-ST complex and (*B*) KaiB–KaiC$^{\Delta505}$-ST complex. Black and gray lines correspond to the elution curves of the KaiB–KaiC mixture with and without incubation at 30 °C for 48 h, respectively. Other chromatograms show assembly and disassembly dynamics of the KaiA–KaiB–KaiC-ST ternary complex after the addition of KaiA at t = 0 h. Peaks labeled "B," "C," "BC," and "ABC" with arrows correspond to the elution peaks of free KaiB, free KaiC, KaiB–KaiC complex, and KaiA–KaiB–KaiC complex, respectively. The absorbtion of ultraviolet (UV) in milli-absorbance units (mAU) at a wavelength of 280 nm was monitored. Peak assignments are supported by molecular mass characterization of eluates using multiangle light scattering (*SI Appendix*, Table S4). *A*, *Inset* and *B*, *Inset* show magnified views of peaks corresponding to free KaiB. Time courses for (*C*) phosphorylation, (*D*) ATPase activity, and (*E*) free Kai proteins after the addition of KaiA to the preformed KaiB–KaiC-ST complex (*SI Appendix*, Fig. S3*B*).

Appendix, Fig. S4*E*). Fifth, the KaiA–KaiB–KaiC$^{\Delta505}$-ST complex, which was rarely disassembled and phosphorylated (Fig. 5*B*), could be reproduced when the binding rates of KaiA to the C2 domain of KaiC$^{\Delta505}$-ST were 30- to 50-fold lower than those to the C2 domain of KaiC-ST (*SI Appendix*, Fig. S4*C*). These findings qualitatively support the KaiA-assisted and autocatalytic disassembly of the KaiA–KaiB–KaiC-ST complex through the activation of C1/C2-ATPase.

Discussion

In the presence of KaiA and KaiB, KaiC exhibits circadian rhythms not only in its phosphorylation state (8) but also, in its C1/C2-ATPase activity (11, 12, 19, 32); C1/C2-ATPase activity was inhibited during the phosphorylating phase and conversely, was activated during the dephosphorylating phase (Fig. 1*B*). Our biochemical (Fig. 1 *C* and *D* and *SI Appendix*, Table S3) and structural (Figs. 2 and 3) analyses indicated that both C1-ATPase^{full} and C2-ATPase^{full} were activated or inactivated in a concerted manner (e.g., KaiC-ST vs. KaiC-AA) but sometimes under opposing regulation (e.g., KaiC-ST vs. KaiC-pSpT).

Although our results may emphasize a unidirectional causality from the C2 domain to the C1 domain, we also obtained several clues for an allosteric reversal from the C1 domain to the C2 domain. As listed in *SI Appendix*, Table S3, the R217A substitution in KaiC1 little affected the C1-ATPase^{basal} activity (9.0 ± 0.6 d^{-1} with R217A and 10.4 ± 0.5 d^{-1} without R217A). However, in the full-length KaiC, the effect on the C2-ATPase^{full} activity became pronounced (8.5 ± 1.9 d^{-1} with R217A and −2.2 ± 1.6 d^{-1} without R217A). The tendency of the allosteric reversal is further pronounced in the C2-ATPase^{full} activity under the KaiC-AA background (195 ± 25.7 d^{-1} with R217A and 5.0 ± 2.9 d^{-1} without R217A). It is clear that there exists a bidirectional communication between the C1 and C2 domains.

In this context, it would be important to mention the effect of the E318Q mutation, which was systematically introduced to estimate the contribution of the dual-ATPase activities. Selective suppression of C2-ATPase by the E318Q mutation would result in a longer-lived C2 domain in the ATP-bound state. The analysis to separate the C1/C2 contributions is based on the assumption that such a C2-ATP–bound state affects neither the structure

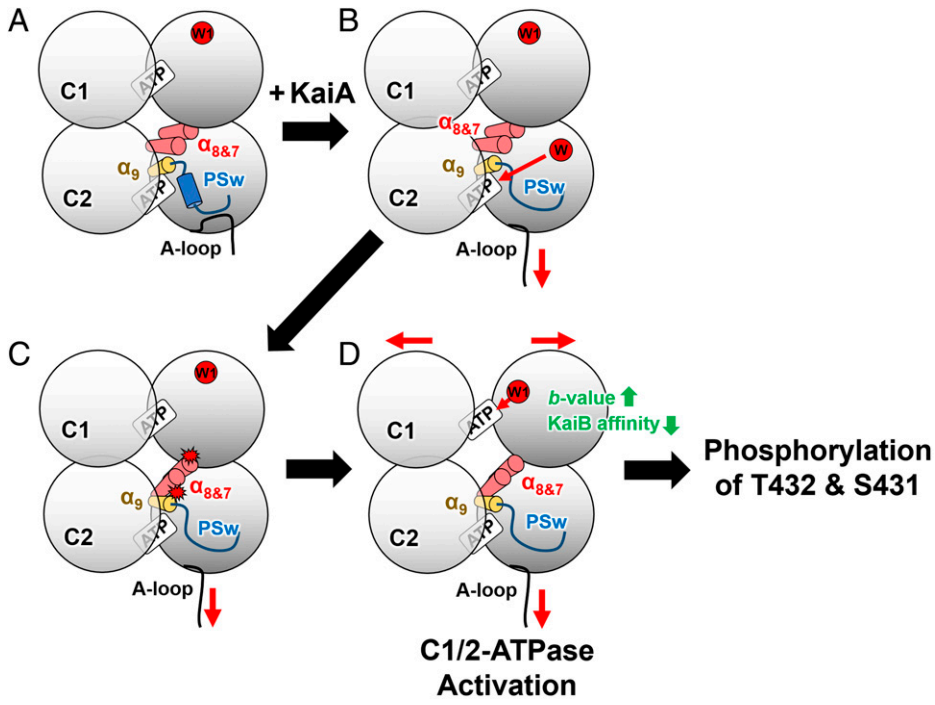

Fig. 6. Schematic drawing of the activation mechanism of the dual ATPase in KaiC-ST. (*A*) KaiC-ST with helical PSw and folded A loop. W1 is sequestered at a position unfavorable for S_N2-type C1-ATP hydrolysis. (*B*) Unfolding of the A loop (24) followed by the helix to coil transition of PSw in KaiA-stimulated KaiC-ST. Bulk water molecules, W, migrate into the C2 active site through the tunnel-shaped void in the C2–C2 interface. (*C*) A short α_9-helix near coiled PSw pushes α_8- and α_7-helices up to the C1 side. (*D*) W1 is relocated to a position much more suitable for C1-ATP hydrolysis through the quaternary structural change of the C1 ring.

nor activity of the C1 domain. While our experimental data indicate that the E318Q substitution has little effect on the overall C1/C2-ATPase activity (Fig. 1*C*), the long-lived C2-ATP–bound state could have some effects on the structure of the C1 domain.

The present results showed that the properties of KaiC-AA were more similar to those of KaiC-ST stimulated by KaiA than to those of unstimulated KaiC-ST. Even in the absence of KaiA, C1-ATPase^{full} and C2-ATPase^{full} of KaiC-AA were both activated to a similar level as when KaiA was added to KaiC-ST (Fig. 1*D*). In contrast to KaiC-ST, PSw of KaiC-AA was coiled (Fig. 4*A*) to form a tunnel-shaped cavity at the C2–C2 interface for bulk water uptake (Fig. 3*C*), and at the same time, W1 was relocated to a suitable position for ATP hydrolysis (Fig. 2*D*) by the quaternary structural change of the C1 ring (Fig. 4*E*). These results suggest that KaiC-AA retains some of the structural and functional features of KaiC-ST stimulated by KaiA.

Assuming that KaiC-AA can be treated as a functional (Fig. 1 *C* and *D*) and structural (Figs. 2*D* and 3*D*) mimic of KaiC-ST stimulated by KaiA, we can infer the results of KaiC-ST activation triggered by KaiA by tracing the conformational change from KaiC-ST to KaiC-AA starting from the KaiA binding site (Fig. 6). The folded A loop hooks the KaiA-binding C terminus (498 to 519) of KaiC-ST, which is in a less exposed configuration (Fig. 6*A*), by a hydrogen bond formed between the main-chain carbonyl oxygen atom of G492 and the main-chain amide of E444 (Fig. 4*A*). This sequence of events begins with KaiA binding to the C-terminal tail of KaiC-ST (25) and drawing out the A loop located on the N-terminal side of the tail (24) (Fig. 6*B*). This induces breaking of the hydrogen bond between G492 and E444, as confirmed in KaiC-AA (Fig. 4*A*). The destabilization of the A loop causes the helix to coil transition of PSw adjacent to the A loop (Fig. 6*B*). Eventually, the tunnel-shaped void at the C2–C2 interface is expanded, and water molecules are taken up through it to the C2-ATPase active site where E318 and C2-ATP are located (Fig. 3). The effect of the structural change in PSw is not confined to the C2 ring but extends to the C1 ring through the C1–C2 interface. The short α_9-helix downstream of PSw moves along its helical axis to the outer-radius side of the hexamer, pushing the α_8- and α_7-helices up to the C1 side (Fig. 6*C*). These perturbations cause a change in the quaternary structure of the C1 domain so that the ring structure expands slightly (Fig. 6*D*); W1 that reacts with C1-ATP is sequestered at the C1–C1 interface via hydrogen bonds between F199 and R226 (F200 and R227 in *Te*KaiC) and is relocated to a position much more suitable for ATP hydrolysis (C1-ATPase) by the change in the C1–C1 interface.

By contrast, the mechanism of inactivating C1-ATPase will be inferred by tracing the conformational change from KaiC-ST to KaiC-pSpT or to KaiC-pST (23). The helix to coil transition of PSw from KaiC-ST to KaiC-pSpT is coupled to the rearrangement of polar residues constituting electrostatic interactions in the C1–C2 interface (23), which causes the tilt and slide movement of the C1 domains to facilitate the quaternary structural change of the C1 ring (Fig. 4*C*). This update of the C1–C1 interface results in W1 sequestration at a position much less suitable for C1-ATP hydrolysis (Fig. 4*E*).

At the same time, it is necessary to mention the possible side effects of the S431A/T432A substitutions. While the changes in the tertiary and quaternary structures (Figs. 3 and 4), as well as the change in the arrangement of W1 (Fig. 2), are intrinsic observations, we cannot rule out the possibility that the expansion of the local cavity around A431/A432 in KaiC-AA is an artificial volume reduction due to the dual alanine substitutions (Fig. 3*D*). Although not limited to this study, amino acid variants designed from a limited number of 19 choices do not always show ideal behaviors reflecting only the intention of

designers and are sometimes accompanied by unexpected side effects due to amino acid substitutions. The validity of our proposal and the need for its update must ultimately be tested by elucidating the complex structure of KaiC-ST and KaiA.

Our results indicate that the activation of dual-KaiC ATPases contributes to a dawn-phase autocatalytic disassembly of the ternary night complexes (Fig. 6 and *SI Appendix*, Fig. S4*F*) and is crucial for resetting subjective night and then pushing the system forward along the unidirectional cycle. Although the structural details of C2-ATPase are still unclear because we were unable to identify the W1s for C2-ATPase, it is simply amazing that it possesses a dynamic range as wide as 0 to 200 d^{-1} (Fig. 1*D* and *SI Appendix*, Table S3). Given that the activity level of C2-ATPase is suppressed to zero in KaiC-ST, its autoinhibitory mechanism and its physiological significance are the next important research targets, which will hopefully lead to a better understanding of the structural and functional roles of the KaiC dual ATPase in the circadian clock system.

Materials and Methods

Expression, Purification, and Crystallization of KaiC. Plasmid vectors for wild-type KaiC, KaiC mutants, and *Te*KaiC were generated for glutathione *S*-transferase–tagged (pGEX-6P-1) (6) or hexahistidine-tagged (pET-3a) (18) forms. Kai proteins were expressed in *Escherichia coli* BL21(DE3) or BL21(DE3)pLysE and purified as reported previously (18, 36).

All crystals were obtained by the vapor diffusion method as reported previously (23). The *Te*KaiC-pSpT crystal in the $P2_12_12_1$ space group was obtained in solutions containing 80 mM acetic acid and 1.0 M sodium acetate and frozen with 25% (wt/vol) polyethylene glycol 8000. The KaiC-AA crystal in the *R*3 space group was obtained in solutions containing 100 mM tris(hydroxymethyl)aminomethane (Tris)·HCl (pH 7.0), 1 M KCl, 0.8 M sodium/potassium tartrate, 0.95 M sodium acetate, and 5 mM adenylyl-imidodiphosphate.

Data Collection and Structure Determination. Preliminary X-ray diffraction experiments were conducted using FRX-Synergy (RIGAKU), and the final dataset was collected on beamline BL44XU at SPring-8 (Harima, Japan) at 100 K under a cryostream. Diffraction images were recorded with an MX-300HE (Rayonix) or PILATUS (Eiger) detector and processed using the HKL2000 (37) and XDSGUI (38) software. Initial phases were determined by molecular replacement methods using structures previously deposited as 2GBL (39) or 4O0M (40) in Protein Data Bank (PDB) and MOLREP (41). Refmac5 (42) and COOT (43) were used to refine and model the crystal structures, respectively. Graphic representations were drawn using PyMOL (Schrödinger). Tunnel-shaped voids were analyzed with a probe radius of 0.6 Å using CAVER 3.0 (44). Statistics of data collection and refinements are listed in *SI Appendix*, Table S1.

Biochemical Assays of Kai Proteins. The four phosphorylation states of KaiC were detected by sodium dodecyl sulfate–polyacrylamide gel electrophoresis and then quantified by LOUPE software (45). The number of ATP molecules hydrolyzed into ADP molecules per KaiC monomer per unit time was quantified at 30 °C as previously described (18, 19). The ATPase activities were analyzed using one-way ANOVA and the Bonferroni post hoc *t* test.

Determination of *b* Values as a Measure of Up- and Down-Regulation of C1-ATPase^{full}. In this study, the ATPase activity of a truncated KaiC consisting solely of the C1 domain (11) was defined as the basal activity (C1-ATPase^{basal}) of C1-ATPase. The ATPase activities of full-length KaiC and its mutants, each of which carries the E318Q substitution that inactivates both kinase and C2-ATPase, were measured to estimate the contribution of C1-ATPase (C1-ATPase^{full}) (*SI Appendix*, Table S3). The *b* value was then calculated as the ratio of C1-ATPase^{full} to C1-ATPase^{basal} using Eq. **1**. The *b* values were analyzed using one-way ANOVA and the Bonferroni post hoc *t* test.

KaiB–KaiC Interaction Assay. KaiB (0.06 mg/mL) was incubated with wild-type KaiC or its mutants (0.3 mg/mL) at 30 °C in a buffer containing 20 mM Tris·HCl (pH 8.0), 150 mM NaCl, 0.5 mM ethylenediaminetetraacetic acid (EDTA), 1 mM ATP, 5 mM $MgCl_2$, and 1 mM dithiothreitol (DTT). Aliquots were taken from the incubated samples after 30 h and subjected to native PAGE analysis (*SI Appendix*, Fig. S3*A*). Electrophoresis was performed at 25 °C using running buffer containing 25 mM Tris·HCl (pH 8.3), 192 mM glycine, 5 mM $MgCl_2$, and 1 mM ATP.

KaiA–KaiB–KaiC Interaction Assay. KaiB and KaiC were mixed in a buffer containing 20 mM Tris·HCl (pH 8.0), 150 mM NaCl, 0.5 mM EDTA, 1 mM ATP, 5 mM $MgCl_2$, and 1 mM DTT and then incubated at 30 °C to equilibrate the formation of the KaiB–KaiC-ST complex. After incubation for 48 h, KaiA was added to the equilibrated KaiB–KaiC-ST mixture at final concentrations of 0.06, 0.06, and 0.3 mg/mL for KaiA, KaiB, and KaiC, respectively (a 1:3:3 molar ratio on a per monomer basis). Every aliquot taken from the KaiA–KaiB–KaiC-ST mixture incubated at 30 °C was subjected to SEC and native PAGE analyses (*SI Appendix*, Fig. S3*B*). A Superdex 200 column (Cytiva) was connected to a multiangle light scattering system (Viscotek TDA305; Malvern) to estimate the molecular masses of the eluted peaks (*SI Appendix*, Table S4). Native PAGE analysis was conducted at 25 °C using running buffer containing 25 mM Tris·HCl (pH 8.3), 192 mM glycine, 5 mM $MgCl_2$, and 1 mM ATP.

Data Availability. Atomic coordinates and structure factors have been deposited in PDB (ID codes 7DY1 [*Te*KaiC] and 7DYE [KaiC-AA]). All other data are included in the manuscript and/or *SI Appendix*.

ACKNOWLEDGMENTS. Diffraction data were collected at BL44XU at the SPring-8 facility under Proposals 2017A6700, 2017B6700, 2018A6700, 2018B6700, 2019A6700, 2019B6700, 2020A6700, 2020A6500, 2017A6702, 2017B6702, 2018A6802, 2018B6802, 2019A6902, 2019B6902, and 2020A6502. This research was partly supported by Platform Project for Supporting Drug Discovery and Life Science Research (Basis for Supporting Innovative Drug Discovery and Life Science Research) from Japan Agency for Medical Research and Development Grant JP20am0101072. This study was supported by Grants-in-Aid for Scientific Research 19K16061 (to Y.F.), 18K06171 (to A.M.), and 17H06165 (to S.A.).

Author affiliations: [a]Research Center of Integrative Molecular Systems, Institute for Molecular Science, National Institutes of Natural Sciences, Okazaki 444-8585, Japan; [b]Department of Functional Molecular Science, The Graduate University for Advanced Studies, Okazaki 444-8585, Japan; [c]Department of Theoretical and Computational Molecular Science, Institute for Molecular Science, National Institutes of Natural Sciences, Okazaki 444-8585, Japan; [d]Department of Biological Science, Division of Natural Science, Graduate school of Science and Institute for Advanced Research, Nagoya University, Nagoya 464-8602, Japan; [e]Institute for Protein Research, Osaka University, Suita 565-0871, Japan; [f]Graduate School of Bioagricultural Sciences, Nagoya University, Nagoya 464-8601, Japan; [g]Institute of Transformative Bio-Molecules, Nagoya University, Nagoya 464-8601, Japan; [h]Graduate School of Life Sciences, Ritsumeikan University, Kusatsu 525-8577, Japan; and [i]College of Life Sciences, Ritsumeikan University, Kusatsu 525-8577, Japan

1. M. Ishiura *et al.*, Expression of a gene cluster kaiABC as a circadian feedback process in cyanobacteria. *Science* **281**, 1519–1523 (1998).
2. S. Akiyama, Structural and dynamic aspects of protein clocks: How can they be so slow and stable? *Cell. Mol. Life Sci.* **69**, 2147–2160 (2012).
3. K. Ito-Miwa, K. Terauchi, T. Kondo, "Mechanism of the cyanobacterial circadian clock protein KaiC to measure 24 hours" in *Circadian Rhythms in Bacteria and Microbiomes*, C. H. Johnson, M. J. Rust, Eds. (Springer International Publishing, Cham, Switzerland, 2021), pp. 79–91.
4. C. L. Partch, Orchestration of circadian timing by macromolecular protein assemblies. *J. Mol. Biol.* **432**, 3426–3448 (2020).
5. R. Pattanayek *et al.*, Visualizing a circadian clock protein: Crystal structure of KaiC and functional insights. *Mol. Cell* **15**, 375–388 (2004).
6. T. Nishiwaki *et al.*, A sequential program of dual phosphorylation of KaiC as a basis for circadian rhythm in cyanobacteria. *EMBO J.* **26**, 4029–4037 (2007).
7. M. J. Rust, J. S. Markson, W. S. Lane, D. S. Fisher, E. K. O'Shea, Ordered phosphorylation governs oscillation of a three-protein circadian clock. *Science* **318**, 809–812 (2007).
8. M. Nakajima *et al.*, Reconstitution of circadian oscillation of cyanobacterial KaiC phosphorylation in vitro. *Science* **308**, 414–415 (2005).
9. T. Nishiwaki, T. Kondo, Circadian autodephosphorylation of cyanobacterial clock protein KaiC occurs via formation of ATP as intermediate. *J. Biol. Chem.* **287**, 18030–18035 (2012).
10. T. Nishiwaki-Ohkawa, Y. Kitayama, E. Ochiai, T. Kondo, Exchange of ADP with ATP in the CII ATPase domain promotes autophosphorylation of cyanobacterial clock protein KaiC. *Proc. Natl. Acad. Sci. U.S.A.* **111**, 4455–4460 (2014).

11. J. Abe *et al.*, Circadian rhythms. Atomic-scale origins of slowness in the cyanobacterial circadian clock. *Science* **349**, 312–316 (2015).
12. K. Terauchi *et al.*, ATPase activity of KaiC determines the basic timing for circadian clock of cyanobacteria. *Proc. Natl. Acad. Sci. U.S.A.* **104**, 16377–16381 (2007).
13. G. Dong *et al.*, Elevated ATPase activity of KaiC applies a circadian checkpoint on cell division in *Synechococcus elongatus*. *Cell* **140**, 529–539 (2010).
14. Y. Kitayama, T. Nishiwaki-Ohkawa, Y. Sugisawa, T. Kondo, KaiC intersubunit communication facilitates robustness of circadian rhythms in cyanobacteria. *Nat. Commun.* **4**, 2897 (2013).
15. C. Phong, J. S. Markson, C. M. Wilhoite, M. J. Rust, Robust and tunable circadian rhythms from differentially sensitive catalytic domains. *Proc. Natl. Acad. Sci. U.S.A.* **110**, 1124–1129 (2013).
16. A. Wiegard *et al.*, *Synechocystis* KaiC3 displays temperature- and KaiB-dependent ATPase activity and is important for growth in darkness. *J. Bacteriol.* **202**, e00478-19 (2020).
17. K. Ito-Miwa, Y. Furuike, S. Akiyama, T. Kondo, Tuning the circadian period of cyanobacteria up to 6.6 days by the single amino acid substitutions in KaiC. *Proc. Natl. Acad. Sci. U.S.A.* **117**, 20926–20931 (2020).
18. D. Ouyang *et al.*, Development and optimization of expression, purification, and ATPase assay of KaiC for medium-throughput screening of circadian clock mutants in cyanobacteria. *Int. J. Mol. Sci.* **20**, 2789–2800 (2019).
19. Y. Murayama *et al.*, Tracking and visualizing the circadian ticking of the cyanobacterial clock protein KaiC in solution. *EMBO J.* **30**, 68–78 (2011).
20. A. Mukaiyama *et al.*, Conformational rearrangements of the C1 ring in KaiC measure the timing of assembly with KaiB. *Sci. Rep.* **8**, 8803 (2018). Correction in: *Sci. Rep.* **10**, 2702 (2020).
21. M. Egli, Architecture and mechanism of the central gear in an ancient molecular timer. *J. R. Soc. Interface* **14**, 20161065 (2017).
22. R. Murakami *et al.*, ATPase activity and its temperature compensation of the cyanobacterial clock protein KaiC. *Genes Cells* **13**, 387–395 (2008).
23. Y. Furuike *et al.*, Elucidation of master allostery essential for circadian clock oscillation in cyanobacteria. *Sci. Adv.* **8**, eabm8990 (2022).
24. Y. I. Kim, G. Dong, C. W. Carruthers Jr., S. S. Golden, A. LiWang, The day/night switch in KaiC, a central oscillator component of the circadian clock of cyanobacteria. *Proc. Natl. Acad. Sci. U.S.A.* **105**, 12825–12830 (2008).
25. I. Vakonakis, A. C. LiWang, Structure of the C-terminal domain of the clock protein KaiA in complex with a KaiC-derived peptide: Implications for KaiC regulation. *Proc. Natl. Acad. Sci. U.S.A.* **101**, 10925–10930 (2004).
26. T. Mori *et al.*, Revealing circadian mechanisms of integration and resilience by visualizing clock proteins working in real time. *Nat. Commun.* **9**, 3245 (2018).
27. Y. Yunoki *et al.*, ATP hydrolysis by KaiC promotes its KaiA binding in the cyanobacterial circadian clock system. *Life Sci. Alliance* **2**, e201900368 (2019).
28. Y. G. Chang *et al.*, Circadian rhythms. A protein fold switch joins the circadian oscillator to clock output in cyanobacteria. *Science* **349**, 324–328 (2015).
29. J. Snijder *et al.*, Insight into cyanobacterial circadian timing from structural details of the KaiB-KaiC interaction. *Proc. Natl. Acad. Sci. U.S.A.* **111**, 1379–1384 (2014).
30. R. Tseng *et al.*, Structural basis of the day-night transition in a bacterial circadian clock. *Science* **355**, 1174–1180 (2017).
31. G. K. Chow *et al.*, Monitoring protein-protein interactions in the cyanobacterial circadian clock in real time via electron paramagnetic resonance spectroscopy. *Biochemistry* **59**, 2387–2400 (2020).
32. A. G. Chavan *et al.*, Reconstitution of an intact clock reveals mechanisms of circadian timekeeping. *Science* **374**, eabd4453 (2021).
33. X. Qin *et al.*, Intermolecular associations determine the dynamics of the circadian KaiABC oscillator. *Proc. Natl. Acad. Sci. U.S.A.* **107**, 14805–14810 (2010).
34. R. Murakami, R. Mutoh, K. Ishii, M. Ishiura, Circadian oscillations of KaiA-KaiC and KaiB-KaiC complex formations in an in vitro reconstituted KaiABC clock oscillator. *Genes Cells* **21**, 890–900 (2016).
35. J. Lin, J. Chew, U. Chockanathan, M. J. Rust, Mixtures of opposing phosphorylations within hexamers precisely time feedback in the cyanobacterial circadian clock. *Proc. Natl. Acad. Sci. U.S.A.* **111**, E3937–E3945 (2014).
36. A. Mukaiyama, D. Ouyang, Y. Furuike, S. Akiyama, KaiC from a cyanobacterium *Gloeocapsa* sp. PCC 7428 retains functional and structural properties required as the core of circadian clock system. *Int. J. Biol. Macromol.* **131**, 67–73 (2019).
37. Z. Otwinowski, W. Minor, Processing of X-ray diffraction data collected in oscillation mode. *Methods Enzymol.* **276**, 307–326 (1997).
38. W. Kabsch, Xds. *Acta Crystallogr. D Biol. Crystallogr.* **66**, 125–132 (2010).
39. R. Pattanayek *et al.*, Analysis of KaiA-KaiC protein interactions in the cyano-bacterial circadian clock using hybrid structural methods. *EMBO J.* **25**, 2017–2028 (2006).
40. R. Pattanayek, Y. Xu, A. Lamichhane, C. H. Johnson, M. Egli, An arginine tetrad as mediator of input-dependent and input-independent ATPases in the clock protein KaiC. *Acta Crystallogr. D Biol. Crystallogr.* **70**, 1375–1390 (2014).
41. A. Vagin, A. Teplyakov, MOLREP: An automated program for molecular replacement. *J. Appl. Crystallogr.* **30**, 1022–1025 (1997).
42. G. N. Murshudov *et al.*, REFMAC5 for the refinement of macromolecular crystal structures. *Acta Crystallogr. D Biol. Crystallogr.* **67**, 355–367 (2011).
43. P. Emsley, B. Lohkamp, W. G. Scott, K. Cowtan, Features and development of Coot. *Acta Crystallogr. D Biol. Crystallogr.* **66**, 486–501 (2010).
44. E. Chovancova *et al.*, CAVER 3.0: A tool for the analysis of transport pathways in dynamic protein structures. *PLOS Comput. Biol.* **8**, e1002708 (2012).
45. Y. Furuike, J. Abe, A. Mukaiyama, S. Akiyama, Accelerating *in vitro* studies on circadian clock systems using an automated sampling device. *Biophys. Physicobiol.* **13**, 235–241 (2016).